An Ultrastable Thiolate/Diglyme Ligated Cluster: Au$_{20}$(PET)$_{15}$(DG)$_2$

An Ultrastable Thiolate/Diglyme Ligated Cluster: Au$_{20}$(PET)$_{15}$(DG)$_2$

Ian D. Anderson,[a] Yuchen Wang,[b] Christine M. Aikens,[b] Christopher J. Ackerson[*a]

The synthesis and characterization of an Au$_{20}$(PET)$_{15}$(DG)$_2$ (PET=phenylethane thiol; DG=Diglyme) cluster is reported. Mass spectrometry reveals this as the first diglyme ligated cluster where diglyme ligands survive ionization into the gas phase. Thermal analysis shows the cluster degrades at 156 °C, whereas the similar Au$_{20}$(PET)$_{16}$ cluster degrades at 125 °C, representing markedly increased thermal stability. A combination of NMR spectroscopy and computational modeling suggests that the diglyme molecules bind in a tridentate manner for this cluster, resulting in a binding energy of 35.2 kcal/mol for diglyme, which is comparable to the value of ~40 kcal/mol for thiolates. IR and optical spectroscopies show no evidence of assembly of this cluster, in contrast to Au$_{20}$(PET)$_{15}$(DG), which readily assembles into dimeric species, which is consistent with a tridentate binding motif. Evidence for stacking among Au-bound and non-bound diglyme molecules is inferred from thermal and mass analysis.

1. Introduction

Atomically-precise thiolate passivated gold nanoclusters represent a sub-set of metal cluster chemistry subject to intense contemporary research.[1] The ease of handling these species relative to other metal clusters enables downstream applications that depend on their robustness. Most work on thiolate protected gold nanoclusters follows the facile Brust-Schiffrin synthesis and related derivatives.[2] The strength of the gold-sulfur bond (~40 kcal/mol) combined with the flexibility of gold[3] has successfully produced a wide array of cluster nuclearities ranging from a few dozen to hundreds of gold atoms.[4–11]

In addition to thiolates, a wide range of ligands such as phosphines, N-heterocyclic carbenes (NHCs), acetylides, and halides are also used to ligate gold clusters.[12–15] Since the ligand shell imparts solubility, stability and reactivity, the introduction of non-thiolate ligands in Brust-type syntheses can produce products with properties inaccessible with thiolate ligands alone.[16–18] Regiochemical control within the ligand shell is also of interest for catalysis, optics, magnetic data storage, bioimaging, theranostics, and sensing applications.[19–21] In particular, studies employing bidentate ligands (e.g. NHCs, diphosphines, dithiolates) have demonstrated a number of advantageous properties such as enhanced optical response, surface rigidity, and self-assembly into larger nanoscale materials.[22–27]

Coordinating solvents can direct syntheses and transformations, sometimes to surprising effect.[28–33] Glycol ethers, more commonly referred to as glymes, are a class of coordinating solvents comprised of saturated non-cyclic polyethers.[34–36] Glymes typically share a myriad of properties[‡] which make them attractive for both research and commercial settings. There remains significant untapped potential in the use of coordinating solvents towards development of simpler formation pathways for mono-functional clusters, which are commonly used in biolabeling.[37] Recent works by Wilson and Owen have demonstrated the size-focusing ability of glymes when applied in the synthesis of lead chalcogenide nanocrystals.[38,39] Incorporation of glymes into the final products were not reported in these cases, however.

Our group has investigated the role of glymes in the synthesis, assembly, and optical properties of gold nanoclusters. We previously found that when diglyme is used as a synthetic co-solvent, it both acts as a size-focusing facilitator and is incorporated as a ligand in the resulting products. In the case of Au$_{20}$(PET)$_{15}$(DG)$_1$, we previously reported a dynamic equilibrium between this cluster monomer and its dimer Au$_{20}$(PET)$_{15}$-DG-Au$_{20}$(PET)$_{15}$.[40] A modified Brust-Schiffrin synthesis in a mixture of diglyme/tetrahydrofuran produced this unique cluster, whose dimerization was mediated by the weak gold-oxygen (~2 kcal/mol) interactions between the cluster surfaces and DG. The dimer dissociation constant was determined to be 20.4 µM. Subsequent femtosecond transient absorption spectroscopic measurements of this dimer revealed distance-dependent intercluster electronic coupling.[41] Increasing the n-glyme length (n = di, tri, tetra) resulted in smaller time constants for electronic relaxation, indicative of stabilization of the dimer-specific excited states.

Our group also synthesized a water-soluble cluster Au$_{25}$(p-MBA)$_{17}$(DG)$_1$ (p-MBA = para-mercaptobenzoic acid), which exhibited diglyme-gold interactions strong enough to resist ligand exchange by incoming thiolates.[42] Unlike Au$_{20}$(PET)$_{15}$(DG)$_1$, there was no evidence for cluster dimers or larger diglyme-connected structures. This was attributed to the

a. *Department of Chemistry, Colorado State University, Fort Collins, CO 80523, USA.*
b. *Department of Chemistry, Kansas State University, Manhattan, KS 66506, USA.*
* ackerson@colostate.edu

enhanced pi-pi stacking ability of PET versus *p*-MBA, as well as steric hindrance and charge repulsion from the carboxylic acid groups on the latter.

One unexplained aspect of prior work using diglyme as a ligand is the question of how exactly diglyme can compete with thiolates in a thiolate-rich environment for ligating a gold cluster surface. Energetically, thiolate binding is markedly preferred. However, some recent work has begun to cast light on oxygen/thiolate ligation competition on gold surfaces. Detailed surface characterization of large (~40 nm) gold colloids by Shumaker-Parry revealed that citrate ligands on gold, instead of a monolayer, stack as chains. This results in a ligand network strong enough to resist displacement by thiolates. Shumaker-Parry concludes that a ligand exchange reaction previously considered highly favourable due to the large difference in gold-sulfur and gold-oxygen bond energies is, in fact, substantially incomplete on citrate passivated gold nanoparticles. This finding is notable because the reaction was widely assumed to be facile and quantitative.[43,44] Similarly, we observed resistance to thiolate-for-diglyme ligand exchange on $Au_{25}(p\text{-MBA})_{17}(DG)_1$.

Building upon prior work with oxygen containing ligands and diglyme as a size-focusing agent, we report here a new heteroleptic diglyme/thiolate ligated $Au_{20}(PET)_{15}(DG)_2$ cluster. The cluster results from a change in our previously disclosed synthesis for diglyme/thiolate ligated $Au_{20}(PET)_{15}(DG)$. Thermal characterization shows this cluster to be remarkably thermally stable. This stability is explained by an NMR spectrum supported computational model that postulates tridentate binding by diglyme to the gold cluster surface. A comparative analysis to previous synthetic studies as well as Shumaker-Parry's findings provides insight into the formation requirements and stability origin of diglyme/thiolate mixed-monolayer clusters.

2. Experimental

2.1 Materials

Gold(III) chloride trihydrate (Sigma-Aldrich, ACS reagent, ≥49.0% Au basis), sodium borohydride (Sigma-Aldrich, ≥98.0% purity), tetra-n-octylammonium bromide (Acros Organics, 98% purity), 2-phenylethanethiol (Sigma-Aldrich, ≥99% purity), diethylene glycol dimethyl ether (diglyme, anhydrous, Sigma-Aldrich, 99.5%), tetrahydrofuran (Fisher Scientific, certified, stabilized with 0.025% butylated hydroxytoluene), dichloromethane (Sigma-Aldrich, ACS grade, ≥99.5%, stabilized with 40-150 ppm amylene), dichloromethane-d₂ (Sigma-Aldrich, 99.5 atom % D), methanol (Fisher Scientific, certified ACS, 99.9% assay), chloroform (EMD Millipore, ≥99.8% assay, stabilized with ethanol), ethanol (Pharmco-Aaper, 200 proof), and DCTB (i.e. trans-2-[3-(4-tert-Butylphenyl)-2-methyl-2-propenyliden]malononitrile, Sigma Aldrich, ≥99.0% [HPLC]) were all used without further purification. Water was obtained using a Thermo Scientific Barnstead Nanopure set to 18.2 MΩ·cm. The synthesis of $[Au_{20}(PET)_{15}(DG)_2]\cdot4[DG]$ was performed based on an adaptation of the conditions from a

previous report.[40] Details on the synthetic conditions can be found within the SI.

2.2 Characterization

MALDI-MS. 2 mg DCTB was dissolved in 200 μL dichloromethane. To this solution was added 2.0 μL of a 10 mg/mL nanocluster sample dissolved in dichloromethane. 0.2 μL of the combined solution was spotted on a stainless steel plate for MALDI-MS and allowed to dry for one hour. Data was collected using a Bruker Microflex LFR MALDI-TOF. Mass spectra were collected in the positive ionization mode, as this consistently gave the best signal-to-noise ratios (versus those collected in negative ionization mode).

NMR. For nanocluster samples, 10 mg was dissolved in 1.0 mL dichloromethane-d₂. For free ligand samples, 100 μL was dissolved in 1.0 mL dichloromethane-d₂. Data was collected using a Bruker Neo400.

TGA. A TA TGA Q500 was used for data collection. Powdered nanocluster (2.0310 mg) was placed in a platinum pan. Under constant N₂ flow (55 mL/min), the temperature was increased at 10 °C/min to 00 °C.

FT-IR. 14.0 mg of nanocluster sample was dissolved in 1.0 mL chloroform, which was measured on a Thermo Nicolet iS-50 FT-IR spectrometer using ATR on a ZnSe crystal.

UV/Vis. 1.0 mL of a 10 mg/mL nanocluster sample dissolved in chloroform was taken and diluted until the absorbance output was within a reasonable range with good signal-to-noise ratio. Data was collected on a NanoDrop 2000c spectrophotometer.

2.3 Computational Details

All calculations were performed at the BP86/TZP[62,63] level of theory with the Grimme3 dispersion correction[64] using the Amsterdam Modeling Suite (AMS) 2021.102 software.[65] After geometry optimization, NMR shielding calculations were performed. ^{1}H NMR calculations were performed on hydrogen atoms in the diglyme molecule with respect to TMS (tetramethyl silane) to be consistent with the experimental results. Further details on these calculations can be found within the SI.

3. Results and Discussion

3.1 Molecular Formula & Diglyme Coordination

Fig. 1 shows the MALDI-MS spectrum of the obtained synthetic product. Full details regarding the synthesis can be found within the SI. In comparison to our previous dimer-monomer synthesis involving $Au_{20}(PET)_{15}(DG)_1$, the major difference is that in this current work reduction with $NaBH_4$ is initiated before dilution with a gross excess of diglyme. The parent peak at 6266 m/z is in excellent agreement with the formula $Au_{20}(PET)_{15}(DG)_2$ (calculated mass: 6266.2 Da). The inset of Fig. 1 shows possible alternative assignments, as well as expected fragments. None of the observed fragments can be associated with the loss of units containing diglyme. This is in notable contrast to the $Au_{20}(PET)_{15}(DG)_1$ monomer-dimer system, wherein the single

ARTICLE
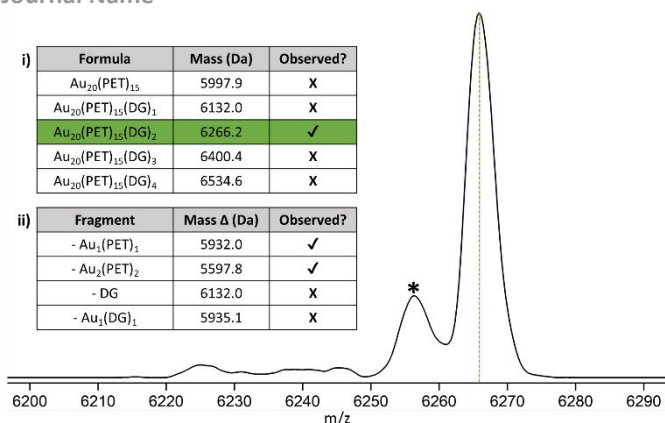
Fig. 1 Positive ion MALDI mass spectrum of the Au_{20} synthetic product, with its parent peak indicated by the green dashed line. Inset table i) lists alternative formulae close in mass to the best match (highlighted in green). Inset table ii) lists potential fragments of primary interest. The label * refers to a combination fragment/adduct peak related to $Au_{20}(PET)_{15}(DG)_2$.

diglyme is bound too weakly to remain bound to the intact cluster under MALDI conditions.[40]

NMR spectroscopy is a powerful analytical tool for clusters in providing evidence of purity, structure, dynamic surface interactions, and magnetism at high spectral resolution.[45–50] **Fig. 2** shows the ^{1}H NMR spectrum of the cluster sample versus that of unbound PET and DG. The broadening of peaks is characteristic of ligands closely associated with a gold cluster surface. This suggests a ligation-type interaction for both PET and DG.[45]

The cluster preparation was washed extensively with excess methanol. Because diglyme is miscible in methanol, we expect any diglyme that is not cluster-associated will be removed. Despite this, peak magnitudes for DG are similar to those for the ethylene linker of PET. Furthermore, the ethylene linker protons are shifted downfield by approximately 0.3 ppm from the chemical shift observed for a comparable fully-thiolated gold cluster, $Au_{25}(PET)_{18}$ (Fig. S1). We attribute this de-shielding effect to the surface-bound DG causing a lowering of the overall electron density on the ethylene linker through the shared gold surface. Intriguingly, the PET phenyl ring protons remain in the
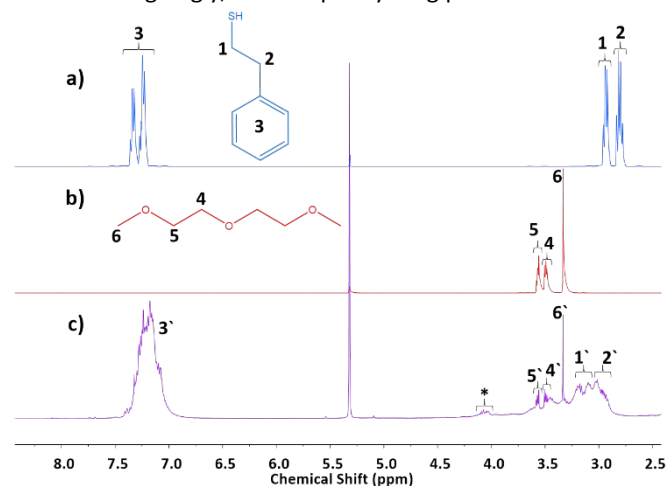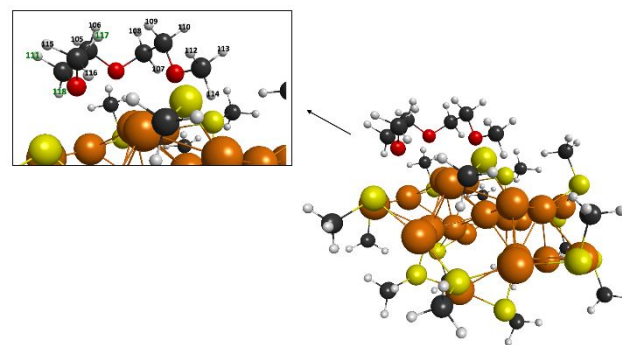
same relative position as those on the surface of $Au_{25}(PET)_{18}$. Combined, these data suggest that the ligated DG is interacting more closely with the ethylene linker than the phenyl ring.

Because the cluster product fails to crystallize (facilitating total structure determination), we computationally modelled several possible structures of a $Au_{20}(SCH_3)_{15}DG$ model system. Models were based initially on the $Au_{20}(PET)_{16}$ crystal structure,[51] with the ligands simplified from -PET to -SCH$_3$. This simplification is justified because the primary goal of the model is to understand the Au-O binding. Calculations considering the full PET ligand require significantly more computational time, and are not expected to add further insight.

To create ligation space for diglyme, one methanethiol ligand was removed from the structure, creating $Au_{20}(SCH_3)_{15}^+$. Because there are 8 symmetrically unique ligand sites, 8 isomers of the cationic $Au_{20}(SCH_3)_{15}DG^+$ systems were considered. For each starting structure, 3 different orientations of diglyme were considered. Overall, 24 different isomers were optimized; the lowest energy structure is shown in **Fig. 3**, and was used for subsequent analysis/interpretation. Due to the large configurational space, this structure is likely not a global minimum. However, many of the higher energy isomers exhibit similar diglyme bonding, suggesting that the structure in Fig. 3 is representative.

Overall, the diglyme displays a crown-like structure bound to the surface of the gold cluster. **Table 1** displays the ^{1}H NMR shielding calculations performed for all hydrogen atoms within the diglyme molecule. Interaction with the $Au_{20}(SCH_3)_{15}^+$ cluster increases the chemical shifts of several hydrogen atoms in the diglyme molecule. We observe that hydrogen atom 117 has the most upfield chemical shift at 3.79 ppm; this atom is oriented away from the gold nanocluster. Hydrogen atom 118 has the highest chemical shift, which is very downfield (6.81 ppm); this hydrogen atom is oriented towards the Au atoms. Hydrogen atom 111 is connected to the same carbon atom as hydrogen atom 118, but this atom is not oriented towards the gold core. Atom 111 has a calculated chemical shift of 4.43 ppm. Therefore, unlike pure diglyme (Table S1), the chemical shift is not dominated by the proximity to neighbouring oxygen and

Fig. 2 ^{1}H NMR spectra of a) free PET, b) free DG, and c) the Au_{20} synthetic product in CD_2Cl_2 with peak assignments for clarity. Peaks labelled with * appear to correspond with diglyme but cannot be unambiguously assigned.

Fig. 3 The fully optimized BP86/TZP structure for $Au_{20}(SCH_3)_{15}DG^+$. The inset provides a more detailed view of the interface between the cluster surface and diglyme. Atoms 117 and 118 are the two hydrogen atoms with the most upfield and most downfield chemical shifts, respectively. Hydrogen atom 111 is the hydrogen atom which is connected to the same carbon atom as atom 118. Gold = orange, carbon = gray, sulfur = yellow, oxygen = red and hydrogen = white. Coordinates provided in SI.

Table 1 Calculated ^{1}H NMR chemical shifts for the hydrogen atoms of diglyme in Au$_{20}$(SCH$_3$)$_{15}$DG$^+$.

| hydrogen atom	chemical shifts (ppm)
105	5.06
106	3.93
107	4.95
108	4.11
109	4.97
110	3.92
111	4.43
112	4.02
113	3.88
114	5.55
115	4.43
116	4.10
117	3.79
118	6.81

carbon atoms; these atoms do not dominate the chemical shifts nearly as much as the proximity to the Au atoms.

Fig. 4 shows the ^{1}H-^{1}H COSY NMR spectrum of the cluster. We observe no interaction between the phenyl ring protons of PET and the DG protons. However, we observe strong correlation between the PET ethylene linker and DG protons. This suggests that the DG ligands are in a closer vicinity to the ethylene linker than the phenyl ring. Due to the dynamic behaviour of cluster ligand layers in solution,[52–54] we would expect some observable degree of spin-spin coupling between DG and the phenyl ring if DG were ligated in a monodentate fashion. A multidentate arrangement would enhance the overall strength of the gold-diglyme interaction, and the chelating ability of DG and other glymes is well documented.[28,34]

Based on the high signal strength of the DG protons relative to the PET protons from NMR analysis, we hypothesized that more than two diglyme molecules were present per formula unit. In order to test this hypothesis, we performed Thermal Gravimetric Analysis (TGA) on the cluster monomer in dry powdered form. **Fig. 5** shows the TGA curve of the powdered cluster. Differential thermal analysis revealed the precise onset of the two weight loss events (Fig. S2). The final weight % is representative of the proportion of the cluster consisting of gold. Conversely, the total weight % loss should match closely with the proportion consisting of the ligands. Assuming a cluster of formula Au$_{20}$(PET)$_{15}$(DG)$_2$ the ligand loss is equivalent to 37.1%, which is significantly different from the observed total
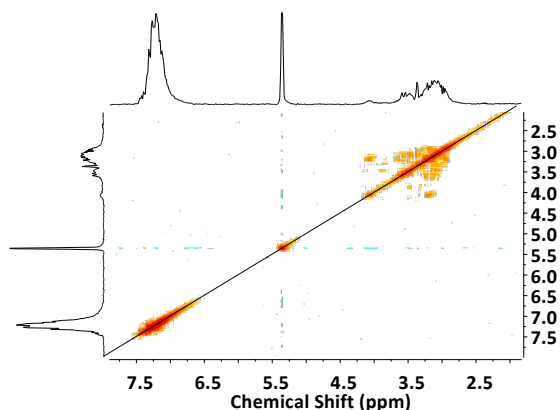
Fig. 4 ^{1}H-^{1}H COSY spectrum of the Au$_{20}$ synthetic product in CD$_2$Cl$_2$. Off-diagonal signal is indicative of spin-spin coupling between different ligand environments.
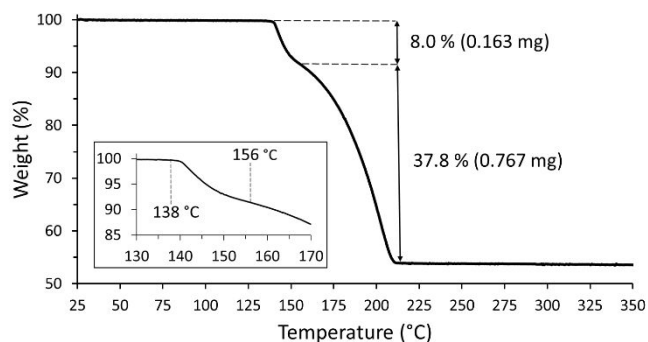
Fig. 5 TGA curve of powdered [Au$_{20}$(PET)$_{15}$(DG)$_2$]·4[DG]. Inset provides a clearer view of the onset temperatures for the two weight loss events.

loss of 45.8%. Furthermore, this formula does not account for the initial weight loss event of 8%.

A significantly better match to the TGA data is obtained by considering the full formula: [Au$_{20}$(PET)$_{15}$(DG)$_2$]·4[DG] (calculated mass: 6803 Da). We propose that this 'excess' diglyme is not directly bound to the gold surface and is therefore easier to remove. The loss of 4 DG molecules is equivalent to a 7.8% loss and the subsequent loss of (PET)$_{15}$(DG)$_2$ is equivalent to 34.2% (total = 42%). It is possible that this 'excess' diglyme is unevenly distributed within the powdered sample, which could help explain the discrepancy between observed and calculated weight loss values.

The onset of decomposition for the all-thiolate Au$_{20}$(PET)$_{16}$ cluster under comparable thermal conditions is at approximately 125 °C.[55] This is considerably lower than [Au$_{20}$(PET)$_{15}$(DG)$_2$]·4[DG], whose inner ligand shell does not desorb until approximately 156 °C. Similarly, Au$_{20}$(PET)$_{15}$-DG-Au$_{20}$(PET)$_{15}$ does not begin to shed its ligand shell until approximately 150 °C.[40] It is therefore evident from both our previous and current work that the coordination of diglyme to thiolate-protected gold nanoclusters results in a significant enhancement of surface stability. The calculated binding energies between Au$_{20}$(SCH$_3$)$_{15}$$^+$ and the first diglyme is around 35.2 kcal/mol (Table S2), which is consistent with the experimental observation for the strong diglyme-gold interaction.

3.2 Optical & Assembly Behaviour

The linear absorption spectrum of [Au$_{20}$(PET)$_{15}$(DG)$_2$]·4[DG] is comprised of a single broad peak centered at 512 nm (Fig. S3). This is less complex than the absorption spectra of Au$_{20}$(PET)$_{16}$ and Au$_{20}$(PET)$_{15}$-DG-Au$_{20}$(PET)$_{15}$, but is similar to Au$_{20}$(PET)$_{15}$(DG)$_1$.[40,55] Based on the presence of multiple diglyme per formula unit and their novel arrangement, we expect electron relaxation dynamics unique from that of the single-diglyme monomer.

Solution-phase FT-IR analysis of the cluster shows a lack of vibrations in the region of 2000-1750 cm^{-1} (Fig. S4). This set of vibrations is observable within the dimer Au$_{20}$(PET)$_{15}$-DG-Au$_{20}$(PET)$_{15}$, arising from strong ligand-layer vibrational coupling between the two Au$_{20}$ monomer units.[40] We find no compelling

evidence for such interactions within this new cluster, therefore establishing it as a purely monomeric species.

$[Au_{20}(PET)_{15}(DG)_2] \cdot 4[DG]$ can be repeatedly dried and re-suspended up to three times without any indication of decomposition. The low vapor pressure and wide liquid range of diglyme appears to help facilitate this degradative resistance. Furthermore, the solution-phase shelf life is remarkable, with no significant decomposition following storage in chloroform at 0 °C for up to 18 months. To test whether $[Au_{20}(PET)_{15}(DG)_2] \cdot 4[DG]$ is capable of hierarchical assembly, we performed a series of heating experiments. Highly-concentrated chloroform solutions of the cluster monomer were set in water baths ranging from 30-60 °C and allowed to equilibrate at each temperature for up to one hour; additional experiments involving a gross excess of diglyme were also conducted (Fig. S5). Overall, we observed no change in the absorption profile of $[Au_{20}(PET)_{15}(DG)_2] \cdot 4[DG]$ over the course of these experiments, demonstrating that it is highly resistant to dimerization/polymerization.

3.3 Glyme-Directed Formation Pathway

Modification of the reducing agent addition step is known to greatly influence the product distribution in Brust-type gold nanocluster syntheses.[56,57] It is also well-known that clusters only begin to form once a significant electron reservoir (i.e. the reducing agent) is introduced. The synthetic conditions to obtain $[Au_{20}(PET)_{15}(DG)_2] \cdot 4[DG]$ are nearly identical to that for the dimer-monomer system, with the exception of this step. As mentioned previously, the dimer-monomer synthesis introduces the reducing agent after diluting the reaction solution with a gross excess of diglyme (523.7 eq relative to $HAuCl_4 \cdot 3H_2O$).[40] Our modified synthesis reverses the order, instead adding the reducing agent prior to the dilution step. Cluster formation therefore begins with a significantly lower diglyme content: 87.3 eq for $[Au_{20}(PET)_{15}(DG)_2] \cdot 4[DG]$ versus 611 eq in the case of the dimer-monomer system. Notably, $Au_{25}(p\text{-}MBA)_{17}(DG)_1$ also formed using a lower diglyme content (74.2 eq).[42] Combined, our results indicate that modification of the diglyme content directly influences the final cluster product identity.

It is interesting that gold-thiolate nanocluster syntheses have a propensity for incorporation of glymes within the final products, unlike in the case of lead chalcogenide nanocrystals where they appear to only control the size.[37,38] We posit that the different predominant formation pathways for lead chalcogenide nanocrystals (nucleation and growth) and gold-thiolate nanoclusters (etching) play a significant role in this difference of outcome. Further mechanistic studies in both of these areas need to be performed in order to fully appreciate the directing role of glymes in synthesis.

3.4 Diglyme Configuration & Apparent Ligand Cross-Linking

Even at the minimum laser intensity, the high energy conditions of MALDI-MS are more than sufficient to ablate weakly-interacting ligands from the surfaces of gold nanoclusters.[49,58] It is remarkable that two molecules of diglyme are strongly bound

enough to remain on the intact cluster. The only other example of such a phenomenon to date is from our own report on $Au_{25}(p\text{-}MBA)_{17}(DG)_1$.[42] In addition, the diglyme-diglyme interactions of $[Au_{20}(PET)_{15}(DG)_2] \cdot 4[DG]$ are notably stronger than the gold-sulfur interactions of the all-thiolate analogue within a thermal decomposition context (desorption at 138 °C versus 125 °C).[55]

As Park and Shumaker-Parry's studies initially revealed, oxygen-containing coordinating ligands can exhibit remarkably strong surface chemistry due to inter-ligand stacking networks.[43,44] In the case of citrates, one of the prominent intermolecular forces was identified as van der Waal attractions between neighbouring chains *via* proximal CH_2 moieties. Our work extends this unique surface chemistry to atomically-precise clusters with glymes.

The strong hydrogen-bond acceptor ability of diglyme is well-documented.[59] Attraction between CH_2 moieties within PET and diglyme is evident from our ^1H-^1H NMR spectral data. Furthermore, the difference in formulation between mass spectrometry and TGA suggests that at least two configurations of diglyme with significantly different binding strengths are at play. Our current working hypothesis is that the 'excess' 4[DG] is stacked in a similar fashion to what is observed in Park and Shumaker-Parry's citrate-capped colloids. Based on the observed lack of correlation with the PET phenyl ring, the specific diglyme stacking arrangement must be 'buried' alongside the ethylene linkers of PET. To our knowledge, this is the first example of such a protecting motif in gold nanoclusters. Assuming an even distribution between the two directly surface-bound diglyme, $[Au_{20}(PET)_{15}(DG)_2] \cdot 4[DG]$ should therefore have two groups of three-diglyme long stacks.

Thus far, $[Au_{20}(PET)_{15}(DG)_2] \cdot 4[DG]$ has proven resistant to hierarchical assembly. This may be due to suboptimal positioning of the outermost diglyme, although the presence of a gross excess of diglyme in our thermal activation study should be able to serve as 'bridges' between adjacent clusters.[40] We posit that the strength of the diglyme-diglyme interaction decreases the further it gets from the cluster surface, eventually reaching a point of diminishing returns which make longer diglyme stacks energetically unfavourable.

One open question which remains is the precise orientation of both the inner DG ligands and the outer excess DG. We have some insight from theory and the ^1H and ^1H-^1H spectra with regard to the former, but this has yet to be unambiguously confirmed through crystallography. Simulated structures of gas-phase bare Au_{20} as well as empirical data on phosphine-protected Au_{20} arrange all gold atoms within a highly stable tetrahedral structure (i.e. all gold is exposed to the surface).[60,61] If true, this would create a scenario wherein up to five gold atoms are not directly coordinated to one of the 15 thiolate ligands, freeing them up for potential chelation with glymes.

Conclusions

The use of coordinating cosolvents such as glymes in Brust-type syntheses is relatively unexplored, and represents a handle for modification of cluster surface chemistry. It is likely that

through careful tuning of reaction conditions, a series of diglyme-ligated gold nanoclusters can be produced. Whether all nuclearities would have enhanced surface stability remains a point of conjecture, as the curvature of the cluster surface necessarily plays a significant role in the orientation of diglyme. For $[Au_{20}(PET)_{15}(DG)_2]\cdot 4[DG]$, post-synthetic modification studies on traditional ligand exchange and intercluster metal/ligand exchange are of immediate interest. If the ligated DG exhibit resistance to exchange by incoming thiolates, a 100% diglyme-protected gold nanocluster may be completely shielded from intercluster exchange (typically a facile process). We anticipate that excited state absorption measurements of this cluster monomer will provide a detailed view of its electronic energy landscape, which may help to explain its resistance to hierarchical assembly. X-ray absorption experiments could offer more insight into the various coordination environments unique to this cluster, if a crystal structure is not forthcoming. The strong stabilizing effect of diglyme, in addition to the myriad existing research and commercial applications of glymes, makes heteroleptic clusters such as $[Au_{20}(PET)_{15}(DG)_2]\cdot 4[DG]$ exceptional models with which to probe glyme-cluster interactions with atomic precision.

Author Contributions

With assistance in conceptualization and methodology from C.J.A., I.D.A. conducted the nanocluster synthesis, characterization, experimental data analysis, and writing of the original draft. Y.W. produced the NMR calculations and subsequent theoretical data analysis with assistance from C.M.A. All authors were involved in review and editing of the final draft.

Conflicts of interest

There are no conflicts to declare.

Acknowledgements

Notes and references

‡Glymes have miscibility with both water and various organic solvents; a wide liquid range (> 200 °C); low viscosity; high chemical/thermal stability; relatively low vapor pressure and low toxicity (versus common organic solvents). Cleaning products, inks, adhesives, coatings, batteries, and pharmaceutical formulations are among some of the many products for which glymes have already seen use in.

1 M. C. Daniel and D. Astruc, *Chem. Rev.*, 2004, **104**, 293-346.
2 M. Brust, M. Walker, D. Bethell, D. J. Schiffrin, and R. Whyman, *J. Chem. Soc. Chem. Commun.*, 1994, **7**, 801-802.
3 D. M. P. Mingos, *J. Chem. Soc. Dalton*, 1996, **5**, 561–566.
4 Y. Xue, X. Li, H. Li, and W. Zhang, *Nat. Commun.*, 2014, **5**, 4348.
5 Q. Yao, T. Chen, X. Yuan, and J. Xie, *Acc. Chem. Res.*, 2018, **51**, 1338-1348.
6 P. R. Nimmala, B. Yoon, R. L. Whetten, U. Landman, and A. Dass, *J. Phys. Chem. A*, 2013, **117**, 504-517.
7 K. M. Ø. Jensen, P. Juhas, M. A. Tofanelli, C. L. Heinecke, G. Vaughan, C. J. Ackerson, and S. J. L. Billinge, *Nat. Commun.*, 2016, **7**, 11859.
8 S. Yamazoe, S. Takano, W. Kurashige, T. Yokoyama, K. Nitta, Y. Negishi, and T. Tsukuda, *Nat. Commun.*, 2016, **7**, 10414.
9 R. Yang, D. M. Chevrier, C. Zeng, R. Jin, and P. Zhang, *Can. J. Chem.*, 2017, **95**, 1220-1224.
10 S. Kenzler, C. Schrenk, A. R. Frojd, H. Häkkinen, A. Z. Clayborne, and A. Schnepf, *Chem. Commun.*, 2018, **54**, 248-251.
11 N. A. Sakthivel, M. Stener, L. Sementa, A. Fortunelli, G. Ramakrishna, and A. Dass, *J. Phys. Chem. Lett.*, 2018, **9**, 1295-1300.
12 Q. F. Zhang, P. G. Williard, and L. S. Wang, *Small*, 2016, **12**, 2518-2525.
13 K. Salorinne, R. W. Y. Man, P. Lummis, M. S. A. Hazer, S. Malola, J. C. H. Yim, A. J. Veinot, W. Zhou, H. Häkkinen, M. Nambo, and C. M. Crudden, *Chem. Commun.*, 2020, **56**, 6102-6105.
14 Z. Lei, X. K. Wan, S. F. Yuan, Z. J. Guan, and Q. M. Wang, *Acc. Chem. Res.*, 2018, **51**, 2465-2474.
15 J. Q. Goh, S. Malola, H. Häkkinen, and J. Akola, *J. Phys. Chem. C*, 2013, **117**, 22079-22086.
16 P. Maity, H. Tsunoyama, M. Yamauchi, S. Xie, and T. Tsukuda, *J. Am. Chem. Soc.*, 2011, **133**, 20123-20125.
17 M. R. Narouz, K. M. Osten, P. J. Unsworth, R. W. Y. Man, K. Salorinne, S. Takano, R. Tomihara, S. Kaappa, S. Malola, C. T. Dinh, J. D. Padmos, K. Ayoo, P. J. Garrett, M. Nambo, J. H. Horton, E. H. Sargent, H. Häkkinen, T. Tsukuda, and C. M. Crudden, *Nat. Chem.*, 2019, **11**, 419-425.
18 C. A. Hosier, I. D. Anderson, and C. J. Ackerson, *Nanoscale*, 2020, **12**, 6239-6242.
19 R. Jin, C. Zeng, M. Zhou, and Y. Chen, *Chem. Rev.*, 2016, **116**, 10346-10413.
20 C. J. Ackerson, R. D. Powell, and J. F. Hainfeld, *Methods Enzymol.*, 2010, **481**, 195-230.
21 W. Fei, S. Antonello, T. Dainese, A. Dolmella, M. Lahtinen, K. Rissanen, A. Venzo, and F. Maran, *J. Am. Chem. Soc.*, 2019, **141**, 16033-16045.
22 H. Shen, S. Xiang, Z. Xu, C. Liu, X. Li, C. Sun, S. Lin, B. K. Teo, and N. Zheng, *Nano Res.*, 2020, **13**, 1908-1911.
23 S. S. Zhang, L. Feng, R. D. Senanayake, C. M. Aikens, X. P. Wang, Q. Q. Zhao, C. H. Tung, and D. Sun, *Chem. Sci.*, 2018, **9**, 1251-1258.
24 J. Zhang, Y. Zhou, K. Zheng, H. Abroshan, D. R. Kauffman, J. Sun, and G. Li, *Nano Res.*, 2018, **11**, 5787-5798.
25 H. Yao and S. Yaomura, *Langmuir*, 2013, **29**, 6444-6451.
26 S. Knoppe and T. Bürgi, *Phys. Chem. Chem. Phys.*, 2013, **15**, 15816.
27 A. Sels, G. Salassa, S. Pollitt, C. Guglieri, G. Rupprechter, N. Barrabés, and T. Bürgi, *J. Phys. Chem. C*, 2017, **121**, 10919-10926.
28 R. Díaz-Torres and S. Alvarez, *Dalton T.*, 2011, **40**, 10742.
29 Y. F. Hou, B. Liu, K. F. Yue, C. S. Zhou, Y. M. Wang, N. Yan, and Y. Y. Wang, *CrystEngComm*, 2014, **16**, 9560-9567.
30 W. Q. Zhang, W. Y. Zhang, R. D. Wang, C. Y. Ren, Q. Q. Li, Y. P. Fan, B. Liu, P. Liu, and Y. Y. Wang, *Cryst. Growth Des.*, 2017, **17**, 517-526.

ARTICLE

31 H. Yang, F. Cao, D. Li, S. Zeng, Y. Song, and J. Dou, *Dalton T.*, 2015, **44**, 6620-6629.

32 S. Suckert, L. S. Germann, R. E. Dinnebier, J. Werner, and C. Näther, *Crystals*, 2016, **6**, 38.

33 Y. P. Budiman, A. Jayaraman, A. Friedrich, F. Kerner, U. Radius, and T. B. Marder, *J. Am. Chem. Soc.*, 2020, **142**, 6036-6050.

34 S. Tang and H. Zhao, *RSC Adv.*, 2014, **4**, 11251-11287.

35 B. Fleming and S. Rushworth, *J. Sol-Gel Sci. Technol.*, 2017, **82**, 308-314.

36 K. Kim and H. Lee, *Energy Technol.*, 2019, **7**, 1900857.

37 C. L. Heinecke and C. J. Ackerson, *Nanoimaging: Methods and Protocols*, Methods in Molecular Biology, Humana Press: Totowa, NJ, 2013, pp 293-311.

38 P. B. Green, Z. Wang, P. Sohn, C. J. Imperiale, O. Voznyy, and M. W. B. Wilson, *J. Mater. Chem. C*, 2020, **8**, 12068-12074.

39 M. P. Campos, M. P. Hendricks, A. N. Beecher, W. Walravens, R. A. Swain, G. T. Cleveland, Z. Hens, M. Y. Sfeir, and J. S. Owen, *J. Am. Chem. Soc.*, 2017, **139**, 2296-2305.

40 W. S. Compel, O. A. Wong, X. Chen, C. Yi, R. Geiss, H. Häkkinen, K. L. Knappenberger, and C. J. Ackerson, *ACS Nano*, 2015, **9**, 11690-11698.

41 P. J. Herbert, C. Yi, W. S. Compel, C. J. Ackerson, and K. L. Knappenberger, *J. Phys. Chem. C*, 2018, **122**, 19251-19258.

42 J. Armstrong and C. J. Ackerson, *Molecules*, 2021, **26**, 2562.

43 J. W. Park and J. S. Shumaker-Parry, *J. Am. Chem. Soc.*, 2014, **136**, 1907-1921.

44 J. W. Park and J. S. Shumaker-Parry, *ACS Nano*, 2015, **9**, 1665-1682.

45 Z. Wu, C. Gayathri, R. R. Gil, and R. Jin, *J. Am. Chem. Soc.*, 2009, **131**, 6535-6542.

46 H. Qian, M. Zhu, C. Gayathri, R. R. Gil, and R. Jin, *ACS Nano*, 2011, **5**, 8935-8942.

47 K. Salorinne, S. Malola, O. A. Wong, C. D. Rithner, X. Chen, C. J. Ackerson, and H. Häkkinen, *Nat. Commun.*, 2016, **7**, 10401.

48 G. Salassa and T. Bürgi, *Nanoscale Horiz.*, 2018, **3**, 457-463.

49 A. W. Cook and T. W. Hayton, *Acc. Chem. Res.*, 2018, **51**, 2456-2464.

50 R. Zheng, G. M. Bevacqua, N. R. Young, T. C. Allison, and Y. J. Tong, *J. Phys. Chem. A*, 2020, **124**, 7464-7469.

51 C. Zeng, C. Liu, Y. Chen, N. L. Rosi, and R. Jin, *J. Am. Chem. Soc.*, 2014, **136**, 11922-11925.

52 G. Salassa, A. Sels, F. Mancin, and T. Bürgi, *ACS Nano*, 2017, **11**, 12609-12614.

53 M. J. Hostetler, A. C. Templeton, and R. W. Murray, *Langmuir*, 1999, **15**, 3782-3789.

54 R. H. Terrill, T. A. Postlethwaite, C. Chen, C. D. Poon, A. Terzis, A. Chen, J. E. Hutchison, M. R. Clark, and G. Wignall, *J. Am. Chem. Soc.*, 1995, **117**, 12537-12548.

55 M. Zhu, H. Qian, and R. Jin, *J. Am. Chem. Soc.*, 2009, **131**, 7220-7221.

56 Z. Wu, M. A. MacDonald, J. Chen, P. Zhang, and R. Jin, *J. Am. Chem. Soc.*, 2011, **133**, 9670-9673.

57 T. Chen, Q. Yao, Y. Cao, and J. Xie, *Cell Reports Physical Science*, 2020, **1**, 100206.

58 Y. Lu and W. Chen, *Anal. Chem.*, 2015, **87**, 10659-10667.

59 I. T. Rakipov, K. N. Semenov, A. A. Petrov, A. A. Akhmadiyarov, A. A. Khachatrian, A. R. Fakhurtdinova, and B. N. Solomonov, *Thermochimica Acta*, 2021, **700**, 178932.

60 K. Wu, J. Li, and C. Lin, *Chem. Phys. Lett.*, 2004, **388**, 353-357.

61 H. F. Zhang, M. Stender, R. Zhang, C. Wang, J. Li, and L. S. Wang, *J. Phys. Chem. B*, 2004, **108**, 12259-12263.

62 J. P. Perdew, *Phys. Rev. B*, 1986, **33**, 8822-8824.

63 A. D. Becke, *Phys. Rev. A*, 1988, **38**, 3098-3100.

64 S. Grimme, S. Ehrlich, and L. Goerigk, *J. Comput. Chem.*, 2011, **32**, 1456-1465.

65 G. te Velde, F. M. Bickelhaupt, E. J. Baerends, C. F. Guerra, S. J. A. van Gisbergen, J. G. Snijders, and T. Ziegler, *J. Comput. Chem.*, 2001, **22**, 931-967.